HHS Public Access

Author manuscript

AJNR Am J Neuroradiol. Author manuscript; available in PMC 2017 January 01.

Published in final edited form as:

AJNR Am J Neuroradiol. 2016 July ; 37(7): 1216–1222. doi:10.3174/ajnr.A4714.

Mapping the Orientation of White Matter Fiber Bundles: A Comparative Study between Diffusion Tensor Imaging (DTI), Diffusional Kurtosis Imaging (DKI), and Diffusion Spectrum Imaging (DSI)

G. Russell Glenn[a,b,c], **Li-Wei Kuo**[d,*], **Yi-Ping Chao**[e], **Chu-Yu Lee**[a,c], **Joseph A. Helpern**[a,b,c], and **Jens H. Jensen**[a,c,†]

[a]Center for Biomedical Imaging, Medical University of South Carolina, Charleston, South Carolina, USA.

[b]Department of Neurosciences, Medical University of South Carolina, Charleston, South Carolina, USA.

[c]Department of Radiology and Radiological Science, Medical University of South Carolina, Charleston, South Carolina, USA.

[d]Institute of Biomedical Engineering and Nanomedicine, National Health Research Institutes, Miaoli County, Taiwan

[e]Graduate Institute of Medical Mechatronics, Chang Gung University, Taoyuan, Taiwan

Abstract

Background and Purpose—White matter fiber tractography relies on fiber bundle orientation estimates from diffusion MRI. However, clinically feasible techniques such as DTI and DKI utilize assumptions, which may introduce error into *in vivo* orientation estimates. In this study, fiber bundle orientations from DTI and DKI are compared to DSI as a gold standard to assess the performance of each technique.

Materials and Methods—For each subject, full DTI, DKI, and DSI datasets were acquired during two independent sessions, and fiber bundle orientations were estimated using the specific theoretical assumptions of each technique. Angular variability and angular error measures were assessed by comparing the orientation estimates. Tractography generated with each of the three reconstructions was also examined and contrasted.

Results—Orientation estimates from all three techniques had comparable angular reproducibility, but DKI decreased angular error throughout the white matter compared to DTI. DSI and DKI enabled the detection of crossing fiber bundles, which had pronounced effects on tractography relative to DTI. DSI had the highest sensitivity for detecting crossing fibers; however, the DSI and DKI tracts were qualitatively similar.

[†]**Co-corresponding authors at:** Center for Biomedical Imaging, Department of Radiology and Radiological Science, Medical University of South Carolina, 96 Jonathan Lucas, MSC 323, Charleston, SC 29425-0323, USA, jense@musc.edu, Telephone: (843)876-2467 . [*]Institute of Biomedical Engineering and Nanomedicine, National Health Research Institutes, 35 Keyan Rd., Zhunan Town, Miaoli County, Taiwan 35053. lwkuo@nhri.org.tw, Telephone: +886-37-246-166 ext. 37120 .

Conclusion—Fiber bundle orientation estimates from DKI have less systematic error than those from DTI, which can significantly affect tractography. Moreover, tractography obtained with DKI is qualitatively comparable to that of DSI. Since DKI has a shorter typical scan time than DSI, DKI is potentially more suitable for a variety of clinical and research applications.

INTRODUCTION

White matter (WM) fiber tractography is used clinically to visualize functionally important WM tracts and aid neurosurgeons during pre-surgical planning (1,2). Tractography is also an important research tool for studying structural connectivity, as tractography is currently the only non-invasive technique for *in vivo* mapping of anatomical neural connections in the human brain (3). However, tractography relies on fiber bundle orientation estimates derived from particular diffusion MRI (dMRI) techniques, which may suffer from inherent methodological limitations, potentially resulting in clinically misleading information (4,5).

Of the several proposed dMRI methods for estimating the orientation of WM fiber bundles, a common approach utilizes the diffusion orientation distribution function (dODF), which quantifies the relative degree of diffusion mobility along a given direction from physical properties of water diffusion (6-9). Diffusion of water is assumed to be least restricted parallel to the orientation of WM fiber bundles resulting in local maxima of the dODF. The dODF may be defined by:

$$\psi(\boldsymbol{n}) = \frac{1}{z}\int_0^\infty r^\alpha P(r\boldsymbol{n}, t)\, dr,$$

where $\boldsymbol{n}$ is a normalized orientation vector, r is a radial displacement magnitude, $P(\boldsymbol{m}, t)$ is the diffusion displacement probability density function (dPDF) for diffusion displacement $\boldsymbol{m}$ over a diffusion time t, α is a constant radial weighting power, and Z is a normalization constant.

There are several distinct techniques for reconstructing the dODF from dMRI data that differ in their theoretical assumptions and optimal experimental implementation. These include DTI which assumes the diffusion of water can be completely described by Gaussian (normal) diffusion (10-12); diffusional kurtosis imaging (DKI), which extends the DTI model to account for non-Gaussian diffusion effects (13-16); q-ball imaging, which applies the Funk transform to dMRI data from high angular resolution diffusion-weighted imaging (6,7), and diffusion spectrum imaging (DSI) (8,9).

In contrast to other methods, DSI quantifies the dODF by employing an exact (in the narrow gradient pulse limit) Fourier transform relationship between the dMRI signal and the dPDF. To accomplish this requires a dense sampling of q-space with relatively high maximum b-values. In this way, DSI effectively characterizes complex intra-voxel microarchitecture without the need for intricate tissue models or ancillary approximations, although it tends to have more demanding data acquisition requirements than alternative methods. Due to its rigorous mathematical formulation and comprehensive description of intra-voxel diffusion dynamics, DSI may be considered a reference standard for validating of other dODF

techniques for *in vivo* experiments (17). Nonetheless, it should be appreciated that even the exact dODF may not give the precise orientation of WM fiber bundles, reflecting the complex and subtle relationship between diffusion and microstructure.

The DTI dODF contains the same information as the diffusion ellipsoid, and the global maximum of the DTI dODF gives the identical direction as the principal eigenvector of the diffusion tensor (7,16). Although efficient in terms of image acquisition time, DTI is not capable of directly resolving intra-voxel fiber crossings (10-12), which can lead to significant errors in orientation estimates from regions with complex tissue architecture (5,18).

The motivation for considering the kurtosis dODF is twofold. First, there have been a significant number of prior studies employing DKI to investigate neuropathology, including stroke (19-23), Alzheimer's disease (24-28), cancer (29-31), and numerous others. Therefore, a tractography method that is compatible with DKI can be of value. Second, DKI shares some of the practical advantages of DTI that make it particularly attractive for clinical settings, such as small maximum b-values and protocol options with relatively short scan times (14,21,32). For example, in clinical settings, a whole-brain DKI dataset with good image quality may be acquired in approximately 7 minutes (21) and respectable whole-brain DKI tractography has been demonstrated with acquisition times as short as 5.3 minutes (32). Moreover, DKI inherently provides measures of the diffusion and kurtosis tensors, as well as all the corresponding tensor-derived quantitative measures (e.g., mean diffusivity and mean kurtosis), which are of interest for characterizing tissue microstructure (33).

In this study, dODFs derived from DSI, DKI, and DTI using *in vivo* human measurements are directly compared, particularly with regard to their fiber bundle orientation estimates. The errors intrinsic to the dODF orientations from DTI and DKI are calculated utilizing the DSI orientations as benchmarks. In addition, the intra-subject variabilities of dODF orientation estimates are calculated across independent sessions for all three methods. A primary goal of this study is to assess the degree to which the DKI dODF approximates the DSI dODF and improves upon the DTI dODF. Tractography results are also compared qualitatively for the three dODF reconstruction techniques.

METHODS

The study was approved by the institutional review board at our institution, and informed consent was obtained from all participants prior to enrollment in the study. Experiments were performed on 3 healthy volunteers on a 3T MRI system (Tim Trio, Siemens, Erlangen, Germany), and for each participant, 2 full DSI and DKI datasets were obtained, with the DTI dataset being taken as a subset of the DKI dataset. Angular variabilities in the orientation estimates were quantified as the absolute, voxel-wise angular difference for each reconstruction between repeated scans, and for DKI and DTI, angular errors were quantified as the absolute, voxel-wise angular differences from the corresponding DSI scan. For each subject, a T1-weighted magnetization-prepared rapid gradient echo (MPRAGE) images were also acquired for anatomical reference. The experimental design is illustrated in Figure 1, and the angular variability and error measures are illustrated in Figure 2. A detailed

description of our image acquisition protocol and image analysis steps is given in the online supplemental material.

The angular error estimates, as quantified in this study, include contributions from both random and systematic errors. Random error may result from thermal noise, incomplete q-space sampling distributions, and physiological effects such as pulsatile flow and bulk subject motion, while systematic errors arise from the approximations inherent to the DTI and DKI dODFs. Although it is difficult to rigorously isolate the random and systematic components of the angular error, a rough index of systematic error is given by the difference between the angular error and angular variability for a given reconstruction, as the angular variability is a measure of random error. We employed this heuristic approach as a practical means of comparing systematic errors for the DTI and DKI dODFs .

Fiber tracking results were assessed qualitatively by looking at the reconstructed tracts in specific regions with complex fiber bundle geometries and over the whole brain in video provided in the online supplemental material. To aid the qualitative assessment, a color-encoding scheme was employed, where each individual tract was colored by its overall displacement from the starting point to the ending point of the tract, with red indicating a left-right displacement, blue indicating an inferior-superior displacement, and green indicating an anterior-posterior displacement. Similar colors represent similar overall trajectories whereas differing colors indicate tracts following different overall trajectories.

RESULTS

Summary statistics for each subject and ROI are given in Table 1. DTI has the lowest angular variability in both the inclusive and conservative WM ROIs as well as the single fiber bundle ROI, while DSI has the lowest angular variability in both the two and three or more crossing fibers ROI. Conversely, DKI has the highest angular variability in all ROIs, with the exception of the three or more crossing fibers ROI, where DTI has the highest angular variability. However, the angular variabilities for all reconstructions are comparable within each of the ROIs, differing by at most 2.1 degrees in the single fiber bundle ROI (Table 1c). On the other hand, DKI consistently improves angular error compared to DTI in all ROIs. Moreover, the DKI systematic errors are all substantially smaller than the DTI systematic errors, consistent with a higher degree of accuracy for the DKI dODFs.

For the ROIs tested, dODF performance measures are significantly influenced by the fractional anisotropy (FA) value, with the smaller angular variability and angular error for regions with higher FA. Conversely, the occurrence of crossing fibers increased angular variability and angular error in dODF-derived orientation estimates. However, the accuracy of the DKI dODF is less affected than the DTI-derived dODF in crossing fiber regions. Properties of the dODF reconstructions are explored further in the online supplemental material.

To illustrate the group-wise performance of the dODF reconstructions, mean normalized parameter maps are given in Figure 3. All three of the reconstruction techniques demonstrate similar angular variability throughout the WM, but DTI shows improvements in angular

variability in regions with high FA (for example note the corpus callosum and corticospinal tracts in rows 2 and 3, which show high FA contrast). The DKI angular error estimates are relatively consistent throughout the WM, whereas the DTI angular error estimates show distinct WM regions where the angular error deteriorates. In comparing these regions to the normalized FA color maps, it is likely that these regions represent voxels with more complex fiber bundle geometries owing to influences from multiple fiber bundle orientations within a voxel (for example, note the intersecting regions between the corpus callosum and corona radiata which are apparent in rows 1 and 3).

Exemplary tractography results are given in Figure 4. A cross-sectional view of the fiber tracts has been selected to highlight the effects of interactions that occur in regions with complex tissue architecture. This particular slice contains noticeable influences from the corpus callosum, which is mainly oriented along the left-right orientation, and the cortico-spinal tracts (among others), which are mainly oriented along the inferior-superior orientation. This slice also shows effects from the superior longitudinal fasciculus and the cingulum bundle, which are mainly oriented along the anterior-posterior direction. In the tractography panels for DSI and DKI, the corpus callosum can be seen fanning through the corona radiata as it passes from one hemisphere to the next. However, these trajectories are obscured by the DTI dODFs, with the corpus callosum tracts either being prematurely truncated or swept into the corticospinal tracts. It can also be seen from these images that the DSI dODF approximation is more sensitive at detecting multiple peaks (note the extent of the superior longitudinal fasciculus fibers indicated by the white arrows and the predominance of green lobes in the respective 3D dODF renderings). DTI is not capable of directly resolving crossing fibers, which significantly affects tractography through complex regions such as those shown in Figure 4. Full brain tractography results are compared with a video provided in the supplemental material.

DISCUSSION

In this study, we have employed DSI as a reference standard to assess the angular error in orientation estimates from DKI and DTI and quantified the intra-subject angular variability of WM fiber bundle orientation estimates from DTI, DKI, and DSI. We have focused primarily on comparing the estimated fiber orientations that the dODFs identify, as these are the inputs needed for constructing tractography. However, it should be emphasized that these are only approximations for the true fiber orientations, which are in general not known, even if the dODF is measured exactly.

A primary motivation for this study is to help assess the potential of DKI tractography for data obtained with clinical MRI scanners. By estimating both the diffusion and kurtosis tensors, DKI more fully characterizes diffusion in complex neural tissue than conventional DTI, which theoretically should improve tractography. Our experimental results support this proposition, as both the angular and systematic errors are markedly lower for DKI (Table 1, Figure 3). Moreover, tractography generated with DKI is qualitatively much more similar to that obtained with DSI than is DTI tractography (Figure 4). Given that DKI, in comparison to DTI, also provides several additional diffusion measures (e.g., mean kurtosis) that are

sensitive to neuropathological changes associated with a variety of diseases (19-31), there are potentially compelling advantages to DKI vis-à-vis DTI.

Overall, the angular variability estimates are comparable for all three reconstructions in all ROIs, differing by at most 2.1 degrees in the single fiber ROI (Table 1c). However, DKI tends to have increased angular variability compared to both DTI and DSI in all ROIs except for the ROI with three or more crossing fiber bundles. Although the precise origin of this is unclear, DKI's increased angular variability could result from a trade-off between estimation error from incomplete q-space sampling distributions and subject motion, which accumulates over the duration of the scan. DTI, for example, requires the shortest acquisition time, which may result in the lowest contributions of subject motion to angular variability. DSI, on the other hand, uses a large number of diffusion encoding vectors to characterize diffusion dynamics, which could have lower angular variability from the dODF reconstruction but an increased likelihood for subject motion. DKI is also known to be sensitive to reconstruction artifacts resulting from Gibbs ringing (34,35) and noise bias (36), although these are also expected to affect DSI.

In order to acquire high quality, whole-brain DSI and DKI datasets for evaluation, we optimized our protocol for high SNR rather than a short acquisition time. Consequently, the total scan time employed in this study was relatively long in comparison to typical clinical protocols. To improve scan efficiency, one or more of several different strategies may be employed. For example, there have been a number of successful efforts to decrease the q-space sampling burden of DSI, including decreasing the q-space sampling density by sampling fewer points (37,38), sampling only one-half of q-space by assuming symmetry of the q-space data (39,40), or sampling only a quarter of q-space using compressed sensing (41). The acquisition time can also be reduced with multi-slice EPI (42-46), while stronger diffusion encoding gradients can be used to reduce the echo time to improve the SNR (46). Although DSI may show the largest improvement in acquisition time, these considerations are generally applicable to DKI as well. It should be noted, however, that there may be an increase in the angular error and variability if SNR is reduced, as may occur with accelerated acquisition schemes (44), or if sparse q-space sampling schemes are employed (39). Nevertheless, DKI may be presumed to have shorter typical scan times than DSI due to the fact that DKI requires only the second and fourth cumulants of the dPDF (47), while DSI employs the full dPDF with the inherent greater data acquisition burden. A valuable follow-up study would be to quantitatively investigate the differences in the orientation estimates using protocols with acquisition times that are more suitable for routine clinical scanning.

There are a variety of alternative techniques that can resolve the orientations of crossing fiber bundles for tractography. Compared to several other dODF reconstructions, the kurtosis dODF has been shown to have a comparable or improved resolving power (48); however, numerical simulations indicate that the kurtosis dODF may sometimes have a greater angular error than other dODFs for larger fiber crossing angles (16,48). Fiber bundle orientations can also be estimated from directional diffusional kurtosis estimates provided by DKI without estimating the dODF directly (49), or the white matter fiber bundles may be modeled mathematically and used to estimate a model-dependent, fiber orientation distribution function, for example using fiber ball imaging (50) or constrained spherical

deconvolution (51,52). Since none of these techniques is directly analogous to the dODF, they were not included in the present study. In addition, it should be noted that model-based approaches make detailed assumptions about the relationship between WM and the dMRI signal that have yet to be fully validated. Nevertheless, the directional diffusional kurtosis approach has been show to increase fiber detection through the corpus callosum (49), and constrained spherical deconvolution can be highly sensitive to crossing fibers (18,53).

To summarize, in this study we acquired, from 3 healthy volunteers, a unique dataset with 6 full DSI and DKI acquisitions, in order to quantify dODF performance measures from DTI, DKI, and DSI. In general, DKI substantially decreases the error of dODF orientation estimates relative to DTI. Moreover, DKI enables the detection of crossing fibers, which results in pronounced improvements relative to DTI for tractography throughout regions with complex fiber bundle geometries (15,16,32,35). Indeed, our results indicate that the tractography obtained with DKI is qualitatively quite comparable to that for DSI, in spite of DKI sampling a much smaller portion of q-space. With enhanced tractography relative to DTI and shorter typical scan times than DSI, DKI-based tractography is potentially advantageous for a variety of clinical and research applications. However, further studies will be needed to more fully investigate the comparative utility of DKI-based tractography.

CONCLUSION

The higher order information provided by the kurtosis tensor enables DKI to directly resolve crossing fibers and improves the accuracy of DKI relative to DTI for tractography. Both DKI and DTI are capable of mapping the single predominant fiber bundle orientation, but the angular error of DTI deteriorates in regions with complex fiber orientations due to its theoretical limitation under the assumption of Gaussian diffusion. DSI, DKI, and DTI all have comparable angular variabilities; however, DKI has decreased angular error in the dODF fiber orientation estimates relative to DTI. Unlike DTI, DKI is thus able to generate white matter fiber tractography comparable to that of DSI, and due to its shorter typical scan time than DSI, is potentially more suitable for a variety of clinical and research applications.

Supplementary Material

Refer to Web version on PubMed Central for supplementary material.

Acknowledgments

FUNDING

This work was supported by the National Institutes of Health research grant T32GM008716 (to P. Halushka), the Litwin Foundation (to J.A.H.), and grants NHRI-BN-104-PP-06 and MOST-103-2221-E-400-001 (to L.W.K).

DISCLOSURES: Li-Wei Kuo—*RELATED: Grant:* NHRI-BN-104-PP-06*; MOST-103-2221-E-400-001.* **Joseph Helpern—***RELATED: Grant:* Litwin Foundation*; *UNRELATED: Grants/Grants Pending:* NIH.* **Jens Jensen—***RELATED: Grant:* Litwin Foundation,* Comments: I have partial salary support from this grant; UNRELATED: Patents (planned, pending or issued) and Royalties: US Patent 8811706, Comments: I am a co-inventor on a patent that covers one of the imaging methods investigated in our manuscript (DKI). The patent is owned by my former employer (NYU), but I could be entitled to royalities at some point. To date, I have not received royalties from this patent.

*money paid to institution

ABBREVIATIONS

dMRI	diffusion MRI
dPDF	diffusion displacement probability distribution function
dODF	diffusion orientation distribution function
DKI	diffusional kurtosis imaging
DSI	diffusion spectrum imaging
FA	fractional anisotropy
NFD	number of fiber directions
WM	white matter
MPRAGE	magnetization-prepared rapid gradient echo
b0	image in dMRI dataset with no diffusion weighting

REFERENCES

1. Romano A, D'Andrea G, Minniti G, Mastronardi L, Ferrante L, Fantozzi LM, Bozzao A. Pre-surgical planning and MR-tractography utility in brain tumour resection. Eur Radiol. 2009; 19:2798–808. [PubMed: 19533147]
2. Mormina E, Longo M, Arrigo A, Alafaci C, Tomasello F, Calamuneri A, Marino S, Gaeta M, Vinci SL, Granata F. MRI Tractography of Corticospinal Tract and Arcuate Fasciculus in High-Grade Gliomas Performed by Constrained Spherical Deconvolution: Qualitative and Quantitative Analysis. AJNR Am J Neuroradiol. Jun 25.2015 [Epub ahead of print].
3. Lazar M. Mapping brain anatomical connectivity using white matter tractography. NMR Biomed. 2010; 23:821–35. [PubMed: 20886567]
4. Tournier JD, Mori S, Leemans A. Diffusion tensor imaging and beyond. Magn Reson Med. 2011; 65:1532–56. [PubMed: 21469191]
5. Farquharson S, Tournier JD, Calamante F, Fabinyi G, Schneider-Kolsky M, Jackson GD, Connelly A. White matter fiber tractography: why we need to move beyond DTI. J Neurosurg. 2013; 118:1367–77. [PubMed: 23540269]
6. Tuch DS, Reese TG, Wiegell MR, Wedeen VJ. Diffusion MRI of complex neural architecture. Neuron. 2003; 40:885–95. [PubMed: 14659088]
7. Tuch DS. Q-ball imaging. Magn Reson Med. 2004; 52:1358–72. [PubMed: 15562495]
8. Wedeen VJ, Hagmann P, Tseng WY, Reese TG, Weisskoff RM. Mapping complex tissue architecture with diffusion spectrum magnetic resonance imaging. Magn Reson Med. 2005; 54:1377–86. [PubMed: 16247738]
9. Wedeen VJ, Wang RP, Schmahmann JD, Benner T, Tseng WY, Dai G, Pandya DN, Hagmann P, D'Arceuil H, de Crespigny AJ. Diffusion spectrum magnetic resonance imaging (DSI) tractography of crossing fibers. Neuroimage. 2008; 41:1267–77. [PubMed: 18495497]
10. Basser PJ, Mattiello J, Le Bihan D. Estimation of the effective self-diffusion tensor from the NMR spin echo. J Magn Reson. 1994; 103:247–54.
11. Basser PJ, Pierpaoli C. Microstructural and physiological features of tissues elucidated by quantitative-diffusion-tensor-MRI. J Magn Reson. 1996; 111:209–19.
12. Basser PJ, Pajevic S, Pierpaoli C, Duda J, Aldroubi A. In vivo fiber tractography using DT-MRI data. Magn Reson Med. 2000; 44:625–32. [PubMed: 11025519]

13. Jensen JH, Helpern JA, Ramani A, Lu H, Kaczynski K. Diffusional kurtosis imaging: the quantification of non-Gaussian water diffusion by means of magnetic resonance imaging. Magn Reson Med. 2005; 53:1432–40. [PubMed: 15906300]

14. Jensen JH, Helpern JA. MRI quantification of non-Gaussian water diffusion by kurtosis analysis. NMR Biomed. 2010; 23:698–710. [PubMed: 20632416]

15. Lazar M, Jensen JH, Xuan L, Helpern JA. Estimation of the orientation distribution function from diffusional kurtosis imaging. Magn Reson Med. 2008; 60:774–81. [PubMed: 18816827]

16. Jensen JH, Helpern JA, Tabesh A. Leading non-Gaussian corrections for diffusion orientation distribution functions. NMR Biomed. 2014; 27:202–11. [PubMed: 24738143]

17. Hagmann P, Jonasson L, Maeder P, Thiran JP, Wedeen VJ, Meuli R. Understanding diffusion MR imaging techniques: from scalar diffusion-weighted imaging to diffusion tensor imaging and beyond. Radiographics. 2006; 26(Suppl 1):S205–23. [PubMed: 17050517]

18. Jeurissen B, Leemans A, Tournier JD, Jones DK, Sijbers J. Investigating the prevalence of complex fiber configurations in white matter tissue with diffusion magnetic resonance imaging. Hum Brain Mapp. 2013; 34:2747–66. [PubMed: 22611035]

19. Jensen JH, Falangola MF, Hu C, Tabesh A, Rapalino O, Lo C, Helpern JA. Preliminary observations of increased diffusional kurtosis in human brain following recent cerebral infarction. NMR Biomed. 2011; 24:452–7. [PubMed: 20960579]

20. Fung SH, Roccatagliata L, Gonzalez RG, Schaefer PW. MR diffusion imaging in ischemic stroke. Neuroimaging Clin N Am. 2011; 21:345–77. [PubMed: 21640304]

21. Hui ES, Fieremans E, Jensen JH, Tabesh A, Feng W, Bonilha L, Spampinato MV, Adams R, Helpern JA. Stroke assessment with diffusional kurtosis imaging. Stroke. 2012; 43:2968–73. [PubMed: 22933581]

22. Grinberg F, Ciobanu L, Farrher E, Shah NJ. Diffusion kurtosis imaging and log-normal distribution function imaging enhance the visualisation of lesions in animal stroke models. NMR Biomed. 2012; 25:1295–304. [PubMed: 22461260]

23. Umesh Rudrapatna S, Wieloch T, Beirup K, Ruscher K, Mol W, Yanev P, Leemans A, van der Toorn A, Dijkhuizen RM. Can diffusion kurtosis imaging improve the sensitivity and specificity of detecting microstructural alterations in brain tissue chronically after experimental stroke? Comparisons with diffusion tensor imaging and histology. Neuroimage. 2014; 97:363–73. [PubMed: 24742916]

24. Falangola MF, Jensen JH, Tabesh A, Hu C, Deardorff RL, Babb JS, Ferris S, Helpern JA. Non-Gaussian diffusion MRI assessment of brain microstructure in mild cognitive impairment and Alzheimer's disease. Magn Reson Image. 2013; 31:840–6.

25. Benitez A, Fieremans E, Jensen JH, Falangola MF, Tabesh A, Ferris SH, Helpern JA. White matter tract integrity metrics reflect the vulnerability of late-myelinating tracts in Alzheimer's disease. Neuroimage Clin. 2013; 9:64–71. [PubMed: 24319654]

26. Fieremans E, Benitez A, Jensen JH, Falangola MF, Tabesh A, Deardorff RL, Spampinato MV, Babb JS, Novikov DS, Ferris SH, Helpern JA. Novel white matter tract integrity metrics sensitive to Alzheimer disease progression. Am J Neuroradiol. 2013; 34:2105–12. [PubMed: 23764722]

27. Vanhoutte G, Pereson S, Delgado Y, Palacios R, Guns PJ, Asselbergh B, Veraart J, Sijbers J, Verhoye M, Van Broeckhoven C, Van der Linden A. Diffusion kurtosis imaging to detect amyloidosis in an APP/PS1 mouse model for Alzheimer's disease. Magn Reson Med. 2013; 69:1115–21. [PubMed: 23494926]

28. Gong NJ, Wong CS, Chan CC, Leung LM, Chu YC. Correlations between microstructural alterations and severity of cognitive deficiency in Alzheimer's disease and mild cognitive impairment: a diffusional kurtosis imaging study. Magn Reson Imaging. 2013; 31:688–94. [PubMed: 23347602]

29. Raab P, Hattingen E, Franz K, Zanella FE, Lanfermann H. Cerebral gliomas: diffusional kurtosis imaging analysis of microstructural differences. Radiology. 2010; 254:876–81. [PubMed: 20089718]

30. Van Cauter S, Veraart J, Sijbers J, Peeters RR, Himmelreich U, De Keyzer F, Van Gool SW, Van Calenbergh F, De Vleeschouwer S, Van Hecke W, Sunaert S. Gliomas: diffusion kurtosis MR imaging in grading. Radiology. 2012; 263:492–501. [PubMed: 22403168]

31. Rosenkrantz AB, Sigmund EE, Johnson G, Babb JS, Mussi TC, Melamed J, Taneja SS, Lee VS, Jensen JH. Prostate cancer: feasibility and preliminary experience of a diffusional kurtosis model for detection and assessment of aggressiveness of peripheral zone cancer. Radiology. 2012; 264:126–35. [PubMed: 22550312]
32. Glenn GR, Helpern JA, Tabesh A, Jensen JH. Optimization of white matter fiber tractography with diffusional kurtosis imaging. NMR Biomed.
33. Tabesh A, Jensen JH, Ardekani BA, Helpern JA. Estimation of tensors and tensor-derived measures in diffusional kurtosis imaging. Magn Reson Med. 2011; 65:823–36. [PubMed: 21337412]
34. Veraart J, Fieremans E, Jelescu IO, Knoll F, Novikov DS. Gibbs ringing in diffusion MRI. Magn Reson Med. 2015
35. Perrone D, Aelterman J, Pižurica A, Jeurissen B, Philips W, Leemans A. The effect of Gibbs ringing artifacts on measures derived from diffusion MRI. Neuroimage. 2015; 120:441–55. [PubMed: 26142273]
36. Glenn GR, Tabesh A, Jensen JH. A simple noise correction scheme for diffusional kurtosis imaging. Magn Reson Imaging. 2015; 33:124–133. [PubMed: 25172990]
37. Kuo LW, Chen JH, Wedeen VJ, Tseng WY. Optimization of diffusion spectrum imaging and q-ball imaging on clinical MRI system. Neuroimage. 2008; 41:7–18. [PubMed: 18387822]
38. Tefera GB, Zhou Y, Juneja V, Narayana PA. Evaluation of fiber tracking from subsampled q-space data in diffusion spectrum imaging. Magn Reson Imaging. 2013; 31:820–6. [PubMed: 23602724]
39. Kuo LW, Chiang WY, Yeh FC, Wedeen VJ, Tseng WY. Diffusion spectrum MRI using body-centered-cubic and half-sphere sampling schemes. J Neurosci Methods. 2013; 212:143–55. [PubMed: 23059492]
40. Yeh CH, Cho KH, Lin HC, Wang JJ, Lin CP. Reduced encoding diffusion spectrum imaging implemented with a bi-Gaussian model. IEEE Trans Med Imaging. 2008; 27:1415–24. [PubMed: 18815093]
41. Menzel MI, Tan ET, Khare K, Sperl JI, King KF, Tao X, Hardy CJ, Marinelli L. Accelerated diffusion spectrum imaging in the human brain using compressed sensing. Magn Reson Med. 2011; 66:1226–33. [PubMed: 22012686]
42. Feinberg DA, Setsompop K. Ultra-fast MRI of the human brain with simultaneous multi-slice imaging. J Magn Reson. 2013; 229:90–100. [PubMed: 23473893]
43. Larkman DJ, Hajnal JV, Herlihy AH, Coutts GA, Young IR, Ehnholm G. Use of multicoil arrays for separation of signal from multiple slices simultaneously excited. J Magn Reson Imaging. 2001; 13:313–317. [PubMed: 11169840]
44. Setsompop K, Cohen-Adad J, Gagoski BA, Raij T, Yendiki A, Keil B, Wedeen VJ, Wald LL. Improving diffusion MRI using simultaneous multi-slice echo planar imaging. Neuroimage. 2012; 63:569–80. [PubMed: 22732564]
45. Reese TG, Benner T, Wang R, Feinberg DA, Wedeen VJ. Halving imaging time of whole brain diffusion spectrum imaging and diffusion tractography using simultaneous image refocusing in EPI. J Magn Reson Imaging. Mar; 2009 29(3):517–22. [PubMed: 19243032]
46. Setsompop K, Kimmlingen R, Eberlein E, Witzel T, Cohen-Adad J, McNab JA, Keil B, Tisdall MD, Hoecht P, Dietz P, Cauley SF, Tountcheva V, Matschl V, Lenz VH, Heberlein K, Potthast A, Thein H, Van Horn J, Toga A, Schmitt F, Lehne D, Rosen BR, Wedeen V, Wald LL. Pushing the limits of in vivo diffusion MRI for the Human Connectome Project. Neuroimage. 2013; 80:220–33. [PubMed: 23707579]
47. Kiselev, VG. The cumulant expansion: an overarching mathematical framework for understanding diffusion NMR. In: Jones, DK., editor. Diffusion MRI: Theory, Methods and Applications. Oxford University Press; Oxford: 2010. chapter 10
48. Jensen JH, Helpern JA. Resolving power for the diffusion orientation distribution function. Magn Reson Med. 2015 doi: 10.1002. [Epub ahead of print].
49. Neto Henriques R, Correia MM, Nunes RG, Ferreira HA. Exploring the 3D geometry of the diffusion kurtosis tensor-Impact on the development of robust tractography procedures and novel biomarkers. Neuroimage. 2015; 111:85–99. [PubMed: 25676915]
50. Jensen JH, Russell Glenn G, Helpern JA. Fiber ball imaging. Neuroimage. 2016; 124:824–833. [PubMed: 26432187]

51. Tournier JD, Calamante F, Connelly A. Robust determination of the fibre orientation distribution in diffusion MRI: non-negativity constrained super-resolved spherical deconvolution. Neuroimage. 2007; 35:1459–72. [PubMed: 17379540]

52. Tournier JD, Yeh CH, Calamante F, Cho KH, Connelly A, Lin CP. Resolving crossing fibres using constrained spherical deconvolution: validation using diffusion-weighted imaging phantom data. Neuroimage. 2008; 15:617–25. [PubMed: 18583153]

53. Wilkins B, Namgyun L, Niharika G, Law M, Leporé N. Fiber estimation and tractography in diffusion MRI: Development of simulated brain images and comparison of multi-fiber analysis methods at clinical b-values. Neuroimage. 2015; 109:341–56. [PubMed: 25555998]

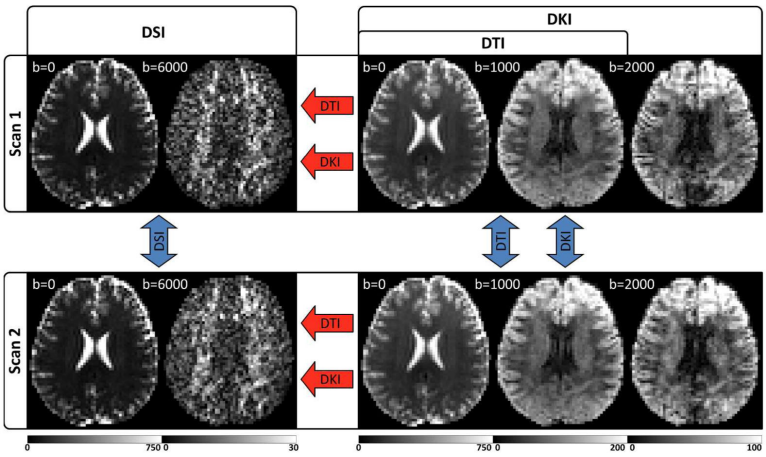

Figure 1.

Experimental design illustrated with example images from a single subject. For each subject, two separate scans are performed, which include independent DSI and DKI acquisitions optimized for the respective reconstructions. The DTI reconstruction is calculated from a subset of the DKI acquisition and is fully independent from the DSI scan but not the DKI scan. Angular variability is calculated between scans (blue arrows) and angular error is calculated for DKI and DTI in reference to the corresponding DSI scan (red arrows). Units for the b-value are s/mm^2, and the signal intensity ranges for each image are given by the corresponding color bar (in arbitrary units). DWIs from the highest b-value for each acquisition are given to illustrate the range of diffusion weighting applied.

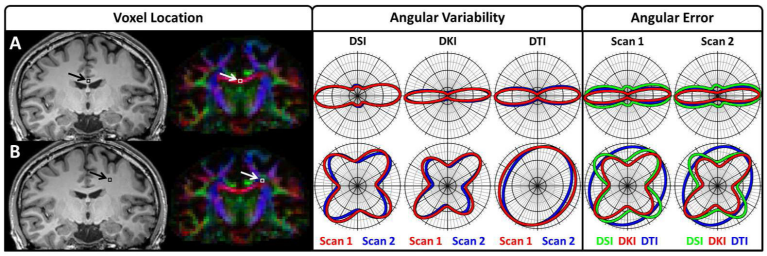

Figure 2.

Polar 2D dODF cross-section plots illustrate angular variability and angular error measures. Row (A) illustrates dODFs taken from a single voxel in the corpus callosum where one predominant fiber bundle orientation is expected, and Row (B) illustrates dODFs taken from a single voxel where multiple fiber bundles are expected to occur between cortical projections from the corpus callosum and ascending and descending fiber bundles in the corona radiata. The Voxel Location tab illustrates the location of the voxels overlaid on the corresponding slice from the MPRAGE image and the FA color map for anatomical reference; the Angular Variability tab illustrates angular variability measures, which are taken between scans for each reconstruction; and the Angular Error tab illustrates the angular error measures, which are taken relative to the corresponding DSI dODF for each scan. The slice plane for the polar plots is rotated to contain the first and second largest orientations of the DSI dODF, as DSI is used as a reference. For visualization, each dODF is scaled to a maximum value of 1.

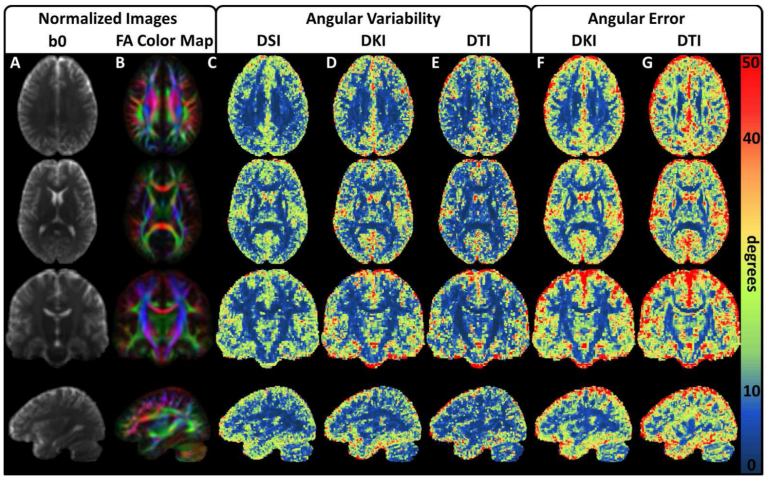

Figure 3.

Group mean angular variability and angular error maps illustrate dODF performance. (A-B) Mean of the normalized b0 and FA color map images, respectively, from all DKI acquisitions. These are included for anatomical reference and to help validate the normalization procedure. The rows illustrate representative transverse, coronal, and sagittal orientations. (C-E) Illustrate angular variability for the DSI, DKI, and DTI reconstructions, respectively. All three techniques demonstrate similar angular variability in the white matter regions. (F,G) Illustrate angular error for the DKI and DTI reconstructions, respectively. Angular error measures increase significantly in regions with low FA, though the angular error for the DKI reconstruction is relatively consistent throughout the WM. The angular error is higher for the DTI reconstruction in the WM, particularly in regions where complex fiber bundle geometries may be present.

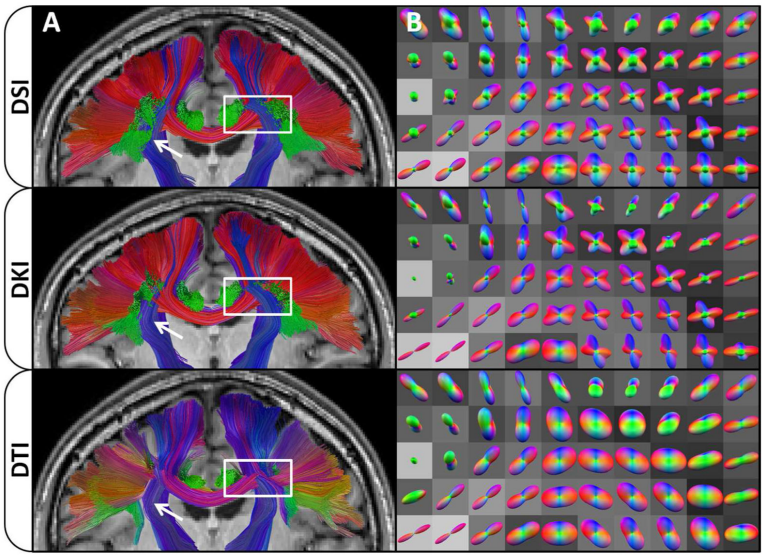

Figure 4.

Effects of dODF reconstructions on WM tractography. Column (A) shows a coronal cross section through the fiber tracts identified with DSI, DKI, and DTI, respectively, overlaid on the corresponding slice from the MPRAGE image for anatomical reference. The color encoding is used to represent the overall displacement of the end points of each tract with one color being applied per tract, where red represents an overall left (L) – right (R) orientation, blue represents an overall inferior (I) – superior (S) orientation, and green represents an overall anterior (A) – posterior orientation. DSI is the most sensitive technique for detecting fibers (white arrows); however, DSI and DKI are fairly similar in both the color, which illustrates the overall trajectory, and distribution of fibers identified. Column (B) shows selected dODFs colored with the same coloring scheme as fibers in column (A), overlaid on the corresponding FA image from the DTI scan. The region shown in Column (B) is demarcated by the white box in the corresponding images in Column (A). DTI fibers are significantly affected in this region, as the dODFs cannot detect crossing fibers causing fibers to prematurely terminate or meld anatomically distinct tracts. This cross section was chosen to demonstrate interactions that occur between the corpus callosum, corona radiata, superior longitudinal fasciculus, and cingulum bundle, and their effects on dODFs and subsequent tractography.

Table 1

dODF performance stats in the FA- and NDF-defined WM ROIs. The number of voxels in each ROI is indicated by n, and values for angular variability and angular error represent the mean (± standard deviation) of the voxel-wise performance measures throughout the ROI. Systematic error is calculated by the difference between the mean angular error and the mean angular varibility over each ROI for the respective reconstructions. All values are given in degrees.

a. Inclusive WM ROI (FA > 0.1)

		Angular Variability			Angular Error		Systematic Error	
	n	DSI	DKI	DTI	DKI	DTI	DKI	DTI
Subject 1	33303	8.7 (9.7)	8.2 (9.4)	7.6 (9.9)	9.9 (10.4)	13.7 (13.8)	1.7	6.1
Subject 2	34087	9.5 (9.7)	9.9 (9.9)	7.7 (9.7)	11.4 (12.3)	14.0 (14.0)	1.4	6.3
Subject 3	35340	6.4 (7.6)	8.3 (9.3)	7.4 (9.3)	10.0 (10.4)	13.8 (14.1)	1.7	6.5
Mean	34243	8.2 (9.0)	8.8 (9.5)	7.6 (9.7)	10.4 (11.0)	13.8 (14.0)	1.6	6.3

b. Conservative WM ROI (FA > 0.3)

		Angular Variability			Angular Error		Systematic Error	
	n	DSI	DKI	DTI	DKI	DTI	DKI	DTI
Subject 1	13692	5.3 (5.7)	4.8 (5.6)	4.4 (5.8)	6.2 (6.6)	10.1 (10.7)	1.4	5.7
Subject 2	11418	5.4 (5.4)	5.8 (5.4)	4.3 (5.6)	6.2 (7.1)	9.4 (10.1)	0.4	5.2
Subject 3	16144	3.7 (4.6)	5.2 (5.7)	4.8 (6.3)	6.3 (6.9)	9.9 (10.7)	1.1	5.0
Mean	13751	4.8 (5.2)	5.3 (5.6)	4.5 (5.9)	6.2 (6.9)	9.8 (10.5)	1.0	5.3

c. Single Fiber ROI (NFD = 1)

		Angular Variability			Angular Error		Systematic Error	
	n	DSI	DKI	DTI	DKI	DTI	DKI	DTI
Subject 1	18808	8.3 (8.3)	7.8 (8.2)	6.4 (7.6)	9.0 (8.7)	10.2 (9.7)	1.2	3.8
Subject 2	18814	8.8 (8.2)	9.2 (8.4)	6.0 (6.4)	10.0 (9.9)	10.5 (9.7)	0.9	4.6
Subject 3	23573	6.3 (7.0)	8.0 (8.4)	6.2 (7.4)	9.4 (9.2)	10.9 (10.8)	1.4	4.7
Mean	20398	7.8 (7.8)	8.3 (8.4)	6.2 (7.1)	9.5 (9.3)	10.6 (10.1)	1.2	4.4

d. Two Crossing Fibers ROI (NFD = 2)

		Angular Variability			Angular Error		Systematic Error	
	n	DSI	DKI	DTI	DKI	DTI	DKI	DTI
Subject 1	11258	9.2 (10.9)	8.7 (10.3)	8.8 (11.5)	10.7 (11.7)	17.4 (16.2)	2.0	8.6
Subject 2	11404	10.0 (10.9)	10.5 (10.8)	9.3 (11.5)	12.4 (13.7)	17.4 (16.2)	1.9	8.1
Subject 3	9824	6.6 (8.6)	8.6 (10.4)	9.2 (11.6)	10.8 (11.8)	18.2 (16.7)	2.2	9.0
Mean	10829	8.6 (10.1)	9.3 (10.5)	9.1 (11.5)	11.3 (12.4)	17.7 (16.4)	2.1	8.6

e. Three or More Crossing Fibers (NFD ≥ 3)

a. Inclusive WM ROI (FA > 0.1)

		Angular Variability			Angular Error		Systematic Error	
	n	**DSI**	**DKI**	**DTI**	**DKI**	**DTI**	**DKI**	**DTI**

		Angular Variability			Angular Error		Systematic Error	
	n	**DSI**	**DKI**	**DTI**	**DKI**	**DTI**	**DKI**	**DTI**
Subject 1	3237	9.7 (12.3)	9.0 (11.7)	10.4 (14.1)	12.6 (14.1)	22.4 (18.9)	3.5	12.0
Subject 2	3869	11.3 (12.4)	12.0 (13.1)	11.4 (14.5)	14.9 (16.6)	21.7 (19.4)	2.9	10.3
Subject 3	1943	7.7 (10.0)	10.1 (12.3)	11.6 (14.0)	13.2 (14.3)	24.8 (19.8)	3.0	13.2
Mean	3016	9.6 (11.6)	10.4 (12.4)	11.1 (14.2)	13.5 (15.0)	23.0 (19.4)	3.2	11.8